

Spin and energy currents in integrable and nonintegrable spin-1/2 chains: A typicality approach to real-time autocorrelations

Robin Steinigeweg,^{1,*} Jochen Gemmer,^{2,†} and Wolfram Brenig^{1,‡}

¹*Institute for Theoretical Physics, Technical University Braunschweig, D-38106 Braunschweig, Germany*

²*Department of Physics, University of Osnabrück, D-49069 Osnabrück, Germany*

(Dated: February 29, 2024)

We use the concept of typicality to study the real-time dynamics of spin and energy currents in spin-1/2 models in one dimension and at nonzero temperatures. These chains are the integrable XXZ chain and a nonintegrable modification due to the presence of a staggered magnetic field oriented in z direction. In the framework of linear response theory, we numerically calculate autocorrelation functions by propagating a single pure state, drawn at random as a typical representative of the full statistical ensemble. By comparing to small-system data from exact diagonalization (ED) and existing short-time data from time-dependent density matrix renormalization group (tDMRG), we show that typicality is satisfied in finite systems over a wide range of temperature and is fulfilled in both, integrable and nonintegrable systems. For the integrable case, we calculate the long-time dynamics of the spin current and extract the spin Drude weight for large systems outside the range of ED. We particularly provide strong evidence that the high-temperature Drude weight vanishes at the isotropic point. For the nonintegrable case, we obtain the full relaxation curve of the energy current and determine the heat conductivity as a function of magnetic field, exchange anisotropy, and temperature.

PACS numbers: 05.60.Gg, 71.27.+a, 75.10.Jm

I. INTRODUCTION

The concept of typicality^{1–11} states that a single pure state can have the same properties as the full statistical ensemble. This concept is not restricted to specific states and applies to the overwhelming majority of all possible states, drawn at random from a high-dimensional Hilbert space. In the cleanest realization, even a single eigenstate of the Hamiltonian may feature the properties of the full equilibrium density matrix, assumed in the well-known eigenstate thermalization hypothesis^{12–14}. The notion of property is manifold in this context and also refers to the expectation values of observables. Remarkably, typicality is not only a static concept and includes the dynamics of expectation values⁷. Recently, it has become clear that typicality even provides the basis for powerful numerical approaches to the dynamics of quantum many-particle systems at nonzero temperatures^{8–11}. These approaches are in the center of this paper.

Understanding relaxation and transport dynamics in quantum many-body systems is certainly one of the most desired and ambitious aims of condensed-matter physics and experiencing an upsurge of interest in recent years, both experimentally and theoretically. On the one hand, the advent of ultracold atomic gases raises challenging questions about the equilibration and thermalization in isolated many-particle systems¹⁵, including the existence, origin, or speed of relaxation processes in the absence of any external bath. On the other hand, future information technologies such as spintronics call for a deeper insight into transport dynamics of quantum degrees of freedom such as spin excitations. Spin transport in conventional nano-systems^{16–19} is inevitably linked to the dynamics of itinerant charge carriers. In contrast, Mott-insulating

quantum magnets allow for pure spin currents and thus open new perspectives in quantum transport. In the past decade, magnetic transport in one-dimensional quantum magnets has attracted considerable attention because of the discovery of very large magnetic heat-conduction^{20–22} and long nuclear magnetic relaxation times^{23,24}. Genuine spin transport, however, still remains to be observed in experiments and particularly its classification in terms of ballistic or diffusive propagation is an issue of ongoing experimental research^{25,26}.

The theoretical study of transport in low-dimensional quantum magnets has a long and fertile history. Amongst all questions, the dissipation of currents is a key issue and has been investigated extensively at zero momentum and frequency in connection with the linear-response Drude weight^{27–39}. The Drude weight is the nondissipating part of the current autocorrelation function and, if existent, indicates a ballistic channel close to equilibrium. While in generic nonintegrable systems it is commonly expected that Drude weights do not exist in the thermodynamic limit³⁵, the picture is different and more complicated in integrable systems: Since an overlap of currents with the macroscopic number of conserved quantities is probable, Drude weights are expected to exist. But this overlap is not necessarily finite for all model parameters and Drude weights can vanish in the thermodynamic limit. In this context, an important example is the antiferromagnetic and anisotropic Heisenberg (XXZ) spin-1/2 chain. This chain is studied in the present paper. It is a fundamental model for the magnetic properties of interacting electrons in low dimensions. It is not only relevant to the physics of one-dimensional quantum magnets⁴⁰ but also to physical questions in a much broader context^{41–44}.

In the XXZ spin-1/2 chain, the heat current is strictly

conserved for all values of the exchange anisotropy Δ ^{27,28} and energy flows through a ballistic channel only. This type of flow is at the heart of the colossal heat conduction observed experimentally in almost ideal material realizations of the model^{20–22}. In contrast, the spin current is not strictly conserved and the existence of a spin Drude weight is a demanding problem, resolved only partially despite much effort. At zero temperature, $T = 0$, early work²⁹ showed that the spin Drude weight is nonzero in the gapless regime $\Delta \leq 1$ (metal) but zero in the gapped regime $\Delta > 1$ (insulator). Bethe-Ansatz solutions^{30,31} support a qualitatively similar picture at nonzero temperatures, $T > 0$, but with a disagreement at the isotropic point $\Delta = 1$. Recent progress in combining quasi-local conservation laws and Mazur’s inequality has lead to a rigorous lower bound to the spin Drude weight in the limit of high temperatures^{32,33}. This bound is very close to the Bethe-Ansatz solution but still allows for a vanishing Drude weight at $\Delta = 1$.

Numerically, a large variety of sophisticated methods has been applied to transport and relaxation dynamics in the anisotropic Heisenberg spin-1/2 chain, including full exact diagonalization (ED)^{34–38,45–47}, $T > 0$ Lanczos methods^{48–50}, quantum Monte-Carlo techniques^{51,52}, as well as time-dependent density matrix renormalization group (tDMRG) approaches to the real-time dynamics of wave packets or correlators^{53–60} and to the solution of the Lindblad quantum master equation^{61,62}. The overwhelming majority of results for the spin Drude weight, however, is only available from ED and tDMRG. Since ED is at present restricted to chains of length $L \sim 20$, the long-time/low-frequency limit is still governed by finite-size effects and intricate extrapolation schemes to the thermodynamic limit have been invoked, with different results depending on details. Such details are using even or odd L ³⁷ and choosing grand-canonical and canonical ensembles⁵⁶. Clearly, these details should be irrelevant in the thermodynamic limit. Alternatively, tDMRG is exceedingly more powerful w.r.t. system size and chains of length $L \sim 200$ are accessible. But still the method is confined to a maximum time scale depending on the exchange anisotropy Δ ^{55–58}. Even though there is an ongoing progress to increase this time scale, it is at present too short for a reliable extraction of the spin Drude weight at the isotropic point $\Delta = 1$ ⁵⁶, which is both, experimentally relevant and theoretically most challenging. In this situation, typicality can provide a fresh numerical perspective⁹.

Much less is known on transport dynamics apart from the mere existence of Drude weights. For spin transport at $\Delta = 1$, steady-state bath scenarios^{61,62} and classical simulations^{63–65} suggest super-diffusive dynamics in the limit of high temperatures, while bosonization predicts diffusion at low but nonzero temperatures⁶⁶. At $\Delta > 1$, signatures of diffusion have been observed also at high temperatures in different approaches^{47,61,62,65,67,68} (see Ref. 57 for a discussion of the limit $\Delta \rightarrow \infty$). Diffusion of heat, however, necessarily requires integrability-breaking

perturbations. For nonintegrable problems, perturbation theory is the only analytical technique available but hard to perform in the thermodynamic limit^{69,70}. The perturbative regime of small integrability-breaking is further challenging for numerical methods since dynamics is slow and physically relevant time scales are long. These long time scales are a challenge for tDMRG and, due to finite-size effects, also for ED. Thus, typicality may complement both numerical methods in this demanding regime.

In this paper, we use the concept of typicality to study the real-time dynamics of spin and energy currents in integrable and nonintegrable spin-1/2 chains at nonzero temperatures. In this way, we extend our previous work in Ref. 10 to energy transport and nonintegrable systems as well. Within the framework of linear response theory, we numerically obtain autocorrelation functions from the propagation of a single pure state, drawn at random as a typical representative of the full statistical ensemble. By comparing to small-system data from ED and existing short-time data from tDMRG, we show that typicality is satisfied in finite systems down to low temperatures and holds in both, integrable and nonintegrable systems. In particular, we demonstrate two numerical advantages of typicality: First, for integrable systems, we can calculate the long-time dynamics and extract the Drude weight for large systems outside the range of ED. Thus, typicality improves the reliability of finite-size scaling. Second, for nonintegrable systems, we can obtain the full relaxation curve for large systems with little finite-size effects on the physically relevant time scale. Hence, typicality provides also the basis for determining the dc conductivity in the regime of small integrability-breaking model parameters without using any fits/extrapolations. Both advantages yield significant progress in the numerical investigation of spin and energy dynamics in particular and of other observables in a much broader context.

This paper is structured as follows: In Sec. II we first introduce the two models studied, namely, the integrable XXZ spin-1/2 chain and a nonintegrable version due to the presence of a staggered magnetic field oriented in z direction. In this Sec. we also define the spin and energy currents, as well as their time-dependent autocorrelation functions, and we discuss symmetries. The next Sec. III is devoted to the concept of dynamical typicality and the closely related numerical technique used throughout this paper. Then we turn to our results: In Sec. IV we focus on spin-current dynamics in the integrable model and study the spin Drude weight as a function of anisotropy and temperature. In the following Sec. V we extend our study in two directions: the nonintegrable model and the dynamics of the energy current. In this Sec. we analyze the dependence of the dc conductivity on magnetic field, anisotropy, and temperature. The last Sec. VI closes with a summary and draws conclusions.

II. MODELS, CURRENTS, AND AUTOCORRELATIONS

A. Integrable Model

In this paper we investigate the antiferromagnetic XXZ spin-1/2 chain. We employ periodic boundary conditions and write the well-known Hamiltonian ($\hbar = 1$)

$$H = \sum_{r=1}^L h_r \quad (1)$$

as a sum over the local energy

$$h_r = J (S_r^x S_{r+1}^x + S_r^y S_{r+1}^y + \Delta S_r^z S_{r+1}^z). \quad (2)$$

S_r^i , $i = x, y, z$ are the components of spin-1/2 operators at site r and L is the total number of sites. $J > 0$ is the antiferromagnetic exchange coupling constant and Δ is the exchange anisotropy in z direction. For $|\Delta| \leq 1$, the model in Eq. (1) has no gap and an antiferromagnetic ground state; for $|\Delta| > 1$, a gap opens and, for $\Delta < -1$, the ground state becomes ferromagnetic^{56,73}.

In general, Eq. (1) is integrable in terms of the Bethe Ansatz^{30,31} and has several symmetries. Two commonly employed symmetries are the invariance under rotation about the z axis, i.e., the conservation of $S^z = \sum_r S_r^z$, and translation invariance. Because of these symmetries, the longitudinal spin $M = -L/2 + i$, $i = 0, 1, \dots, L$ and the momentum $k = 2\pi i/L$, $i = 0, 1, \dots, L-1$ are good quantum numbers. Therefore, the full Hilbert space with $d = 2^L$ states consists of $(2L+1)L$ uncoupled symmetry subspaces with

$$d_{k,M} \approx \frac{1}{L} \binom{L}{|M| + L/2} \quad (3)$$

states, where the largest subspaces have $M = 0$. In this paper we do not restrict ourselves to a specific choice of M or k and take into account all (M, k) subspaces.

Since the longitudinal magnetization S^z and energy H are conserved, their currents are well defined operators and follow from the continuity equation

$$\dot{\rho}_r = i[H, \rho_r] = j_{r-1} - j_r, \quad (4)$$

where ρ_r is either the local magnetization, $\rho_r = S_r^z$, or the local energy, $\rho_r = h_r$, and j_r is the corresponding local current. In case of magnetization, $j_r = -i[S_r^z, h_r]$ and the total current has the well-known form (see, e.g., the review in Ref. 36)

$$j_S = J \sum_{r=1}^L (S_r^x S_{r+1}^y - S_r^y S_{r+1}^x), \quad (5)$$

where the subscript S indicates spin/magnetization for the remainder of this paper. This current commutes with the Hamiltonian only for anisotropy $\Delta = 0$ ³⁶. In the case

of energy, $j_r = -i[h_r, h_{r+1}]$ and the total current can be written as³⁸

$$j_E = J^2 \sum_{r=1}^L [(S_r^x S_{r+2}^y - S_r^y S_{r+2}^x) S_{r+1}^z - \Delta (S_r^x S_{r+1}^y - S_r^y S_{r+1}^x) (S_{r-1}^z + S_{r+2}^z)], \quad (6)$$

where the subscript E indicates energy now. In contrast to the operators in Eqs. (1) and (5), the current in Eq. (6) acts on more than two neighboring sites and involves three adjacent sites. This current and the Hamiltonian commute with each other for all values of Δ ^{27,28}. Both, energy and spin current share the good quantum numbers (M, k) of the Hamiltonian.

B. Nonintegrable Model

To break the integrability of the model, we add to Eq. (1) the term

$$H_B = B \sum_{r=1}^L (-1)^r S_r^z, \quad (7)$$

where B is the strength of a staggered magnetic field oriented in z direction. While this term does not change the above symmetries of the model, we have momentum $k = 2\pi i/(L/2)$, $i = 0, 1, \dots, (L-1)/2$ now and symmetry subspaces are twice as large as before.

Due to the form of H_B , neither the definition of the spin current in Eq. (5) nor the definition of the energy current in Eq. (6) change. In general, j_S is independent of any spatial profile of the magnetic field. But j_E does not change because of the staggered profile of H_B in Eq. (7). A homogenous magnetic field, for instance, yields a magnetothermal correction to the energy current³⁶. Such a correction does not occur in our case. One important consequence of adding H_B is a nonvanishing commutator

$$[H + H_B, j_E] = [H_B, j_E] \propto B \Delta, \quad (8)$$

i.e., the energy current is not strictly conserved for finite values of B and Δ . Note that this commutator also leads to scattering rates $1/\tau \propto (B\Delta)^2$, as discussed in more detail later and in Appendix B.

While the main physical motivation of adding a staggered magnetic field H_B is both, breaking integrability and inducing current scattering, we do not intend to describe a specific experimental situation. Moreover, choosing H_B as perturbation allows us to compare with existing results in the literature.

C. Autocorrelation Functions

Within the framework of linear response theory⁷⁴, we investigate spin and energy autocorrelation functions at

inverse temperatures $\beta = 1/T$ ($k_B = 1$),

$$C_{S/E}(t) = \frac{\text{Re} \langle j_{S/E}(t) j_{S/E} \rangle}{L} = \frac{\text{Re} \text{Tr} \{ e^{-\beta H} j_{S/E}(t) j_{S/E} \}}{L Z}, \quad (9)$$

where the time argument of the operator $j_{S/E}(t)$ has to be understood w.r.t. the Heisenberg picture, $j_{S/E} = j_{S/E}(0)$, and $Z = \text{Tr} \{ \exp(-\beta H) \}$ is the partition function. In the limit of high temperatures $\beta \rightarrow 0$, the sum rules are given by $C_S(0) = J^2/8$ and $C_E(0) = J^4(1 + 2\Delta^2)/32^{27,28}$. Linear response theory describes the dynamics close to equilibrium and is valid in both, integrable and nonintegrable systems^{49,50}. For nonequilibrium effects, see Ref. 49.

Spin and energy autocorrelation functions in Eq. (9) can be written as

$$C_{S/E}(t) = \sum_{k,M} \sum_{n,n'}^{d_{k,M}} \frac{e^{-\beta n}}{Z} \frac{|\langle n | j_{S/E} | n' \rangle|^2}{L} \cos(\omega_{nn'} t), \quad (10)$$

where $n = n(k, M)$ labels eigenstates of the Hamiltonian in the symmetry subspace (k, M) and $\omega_{nn'} = E_n - E_{n'}$ is the difference of eigenvalues E_n and $E_{n'}$. The expression in Eq. (10) provides the basis for exact-diagonalization studies^{34–38,45–47}. In these studies, $C_{S/E}(t)$ can be easily evaluated for arbitrarily long times; however, eigenstates and eigenvalues can be obtained only for systems of finite size. Even with symmetry reduction, accessible sizes are $L \sim 20$ as of today. For such systems, the long-time behavior of $C_{S/E}(t)$ can be affected by strong finite-size effects, also in the limit of high temperatures $\beta \rightarrow 0$. Generally, finite-size effects increase as temperature is lowered and are stronger for integrable systems³⁶.

We are interested in extracting information on two central transport quantities, namely, the Drude weights $\bar{C}_{S/E}$ and the *regular* dc conductivities $\kappa_{S/E}$,

$$\bar{C}_{S/E} = \int_{t_1}^{t_2} dt \frac{C_{S/E}(t)}{t_2 - t_1}, \quad \kappa_{S/E} = \beta \int_0^{t_3} dt C_{S/E}(t). \quad (11)$$

Here, $t_2 \gg t_1 \gg 1/J$, with t_1 and t_2 selected from a region where $C_{S/E}(t)$ has practically decayed to its long-time value $C_{S/E}(t \rightarrow \infty) \geq 0$, which may be zero or nonzero. We emphasize that, with this selection, $\bar{C}_{S/E}$ can be safely viewed as time-independent and is the Drude weight^{27–39}. A nonzero Drude weight exists whenever the current is at least partially conserved and therefore indicates ballistic transport. In cases where the Drude weight vanishes and transport is not ballistic in the thermodynamic limit, the dc conductivities $\kappa_{S/E} = \kappa_{S/E}(\omega \rightarrow 0^+)$ are of interest and result from a zero-frequency Fourier transform of $C_{S/E}(t)$, i.e., the right expression in Eq. (11) with $t_3 \rightarrow \infty$. In finite systems, however, the Drude weight may be tiny but is never zero. Thus, if the limit $t_3 \rightarrow \infty$ is performed in a finite system, $\kappa_{S/E}$ will always diverge. To avoid such divergences for cases with tiny Drude weights, we choose a

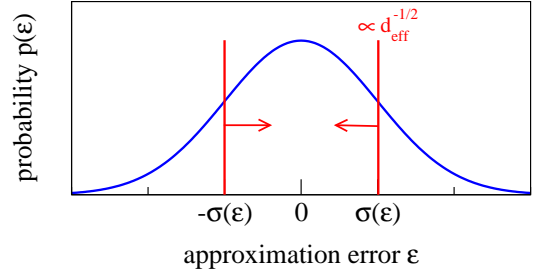


FIG. 1. (color online) Sketch of the probability distribution $p(\epsilon)$ for the approximation error $\epsilon(|\psi\rangle)$ in Eq. (13). While the average of the error vanishes, $\bar{\epsilon} = 0$, the variance of the error decreases as the effective Hilbert-space dimension increases, $\sigma(\epsilon) \propto 1/\sqrt{d_{\text{eff}}}$. This scaling implies that $p(\epsilon)$ is a δ function in the thermodynamic limit.

finite but long cutoff time $t_3 \gg \tau$, where τ is the relaxation time, i.e., $C_{S/E}(\tau)/C_{S/E}(0) = 1/e$. For cases with a clean exponential relaxation, for instance, $t_3 = 5\tau$ is a suitable choice because times $> 5\tau$ do not contribute significantly to $\kappa_{S/E}$. Hence, for these cases, choosing $t_3 = 5\tau$ yields a reasonable approximation of the dc conductivity on the basis of a finite system. In general, one has to ensure that $\kappa_{S/E}$ is approximately independent of the specific choice of t_3 .

Note that other definitions of the Drude weight exist in the literature, where additional prefactors π , 2π , or β appear. Note further that our expression for the energy conductivity is different from other definitions using a prefactor β^2 . In this way, we use the expression in Ref. 59.

III. DYNAMICAL TYPICALITY

A. Approximation

Next we introduce an approximation of autocorrelation functions. This approximation provides the basis of the numerical method used throughout this paper. The central idea amounts to replacing the trace $\text{Tr} \{ \bullet \} = \sum_i \langle i | \bullet | i \rangle$ in Eq. (9) by a single scalar product $\langle \psi | \bullet | \psi \rangle$ involving a pure state $|\psi\rangle$, which, furthermore, is drawn at random. Since we aim at the dynamics in the full Hilbert space, $|\psi\rangle$ is randomly chosen in the full basis. This is conveniently done in the common eigenbasis of symmetries,

$$|\psi\rangle = \sum_{M,k} |\psi_{M,k}\rangle, \quad |\psi_{M,k}\rangle = \sum_s^{d_{M,k}} (a_s + i b_s) |s\rangle, \quad (12)$$

where $s = s(k, M)$ is a label for the common eigenstates of symmetries and a_s, b_s are random real numbers. Specifically, a_s, b_s are chosen according to a Gaussian distribution with zero mean. In this way, the pure state $|\psi\rangle$ is chosen according to a distribution that is invariant

under all unitary transformations in Hilbert space (Haar measure⁷) and, according to typicality¹⁻⁶, a representative of the statistical ensemble.

$|\psi\rangle$ and $|\psi_{M,k}\rangle$ in Eq. (12) correspond to high temperatures $\beta \rightarrow 0$. To incorporate finite temperatures, we introduce $|\psi_{M,k}(\beta)\rangle = \exp(-\beta H/2) |\psi_{M,k}\rangle$. Then, we rewrite the autocorrelation function in Eq. (9) as⁷⁻¹¹

$$C_{S/E}(t) = \frac{\text{Re} \sum_{M,k} \langle \psi_{M,k}(\beta) | j_{S/E}(t) j_{S/E} | \psi_{M,k}(\beta) \rangle}{L \sum_{M,k} \langle \psi_{M,k}(\beta) | \psi_{M,k}(\beta) \rangle} + \epsilon_{S/E}(|\psi\rangle), \quad (13)$$

where $\epsilon_{S/E}(|\psi\rangle)$ encodes the error which results if the first term on the r.h.s. of Eq. (13) is taken as an *approximation* for $C_{S/E}(t)$. This error is random due to the random choice of $|\psi\rangle$. Certainly, one may sample over several $|\psi\rangle$ and in fact $\epsilon_{S/E}$ vanishes, i.e., $\bar{\epsilon}_{S/E} = 0$. This sampling is routinely done to obtain autocorrelation functions in the context of classical mechanics⁶⁵.

The main point of Eq. (13), however, is that, in addition to the mean error $\bar{\epsilon}_{S/E} = 0$, one also knows the standard deviation of errors $\sigma(\epsilon_{S/E})$, as illustrated in Fig. 1. Precisely, one knows an upper bound for $\sigma(\epsilon_{S/E})$ ⁷⁻⁹,

$$\sigma(\epsilon_{S/E}) \leq \mathcal{O} \left(\frac{\sqrt{\text{Re} \langle j_{S/E}(t) j_{S/E} j_{S/E}(t) j_{S/E} \rangle}}{L \sqrt{d_{\text{eff}}}} \right), \quad (14)$$

where d_{eff} , the effective dimension of the Hilbert space, occurs. In the high-temperature limit $\beta \rightarrow 0$, $d_{\text{eff}} = 2^L$ is identical to the full dimension d . Thus, if the number of sites L is increased, $\sigma(\epsilon_{S/E})$ decreases exponentially fast with L . Therefore, remarkably, the *single* pure-state contribution from the first term on the r.h.s. of Eq. (13) turns into an exponentially good approximation for the autocorrelation function. At arbitrary β , $d_{\text{eff}} = \text{Tr}\{\exp[-\beta(H - E_0)]\}$ is the partition function and E_0 the ground-state energy, i.e., d_{eff} essentially is the number of thermally occupied states. Again, this number scales exponentially fast with L^9 but less quickly. To summarize, discarding $\epsilon_{S/E}$ in Eq. (13) is an approximation which is exact in the thermodynamic limit $L \rightarrow \infty$. At finite L , errors can be reduced additionally by sampling, however, this sampling turns out to be unnecessary for all examples in this paper.

B. Numerical Method

The central advantage of the approximation in Eq. (13) is that it can be calculated without the eigenstates and eigenvalues of the Hamiltonian, in contrast to the exact expression in Eq. (10). Specifically, this calculation is based on the two auxiliary pure states

$$|\Phi_{M,k}(\beta, t)\rangle = e^{-iHt - \beta H/2} |\psi_{M,k}\rangle, \quad (15)$$

$$|\varphi_{M,k}(\beta, t)\rangle = e^{-iHt} j_{S/E} e^{-\beta H/2} |\psi_{M,k}\rangle, \quad (16)$$

both depending on time and temperature. Note that the only difference between the two states is the additional

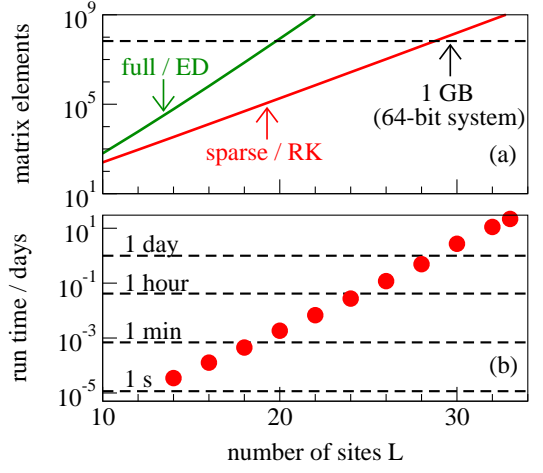


FIG. 2. (color online) (a) Total number of matrix elements required to represent the largest subspaces ($M = 0, k$) of the Hamiltonian in Eq. (1) as a full and sparse matrix. The full matrix for $L = 20$ requires the same amount of computer memory as the sparse matrix for $L = 30$. (b) Run time of the Runge-Kutta algorithm for the same subspaces and the spin current using a single CPU and 10^4 discrete time steps ($\delta t J = 0.01$, $t J = 100$). The run time for $L = 33$ is roughly one month. (Note that adding Eq. (7) to the Hamiltonian increases matrix elements and run time by a factor 2.)

current operator $j_{S/E}$ in the r.h.s. of Eq. (16). By the use of these states, we can rewrite the approximation in Eq. (13) as

$$C_{S/E}(t) = \frac{\text{Re} \sum_{M,k} \langle \Phi_{M,k}(\beta, t) | j_{S/E} | \varphi_{M,k}(\beta, t) \rangle}{L \sum_{M,k} \langle \Phi_{M,k}(\beta, 0) | \Phi_{M,k}(\beta, 0) \rangle}, \quad (17)$$

where we skip the error $\epsilon_{S/E}(|\psi\rangle)$ for clarity. Apparently, a time dependence of the current operator $j_{S/E}$ does not appear anymore in Eq. (17). Instead, the full time and temperature dependence is a property of the pure states only.

The β dependence, e.g. of $|\Phi_{M,k}(\beta, t)\rangle$, is generated by an imaginary-time Schrödinger equation,

$$i \frac{\partial}{\partial(\beta)} |\Phi_{M,k}(\beta, 0)\rangle = \frac{H}{2} |\Phi_{M,k}(\beta, 0)\rangle, \quad (18)$$

and the t dependence by the usual real-time Schrödinger equation,

$$i \frac{\partial}{\partial t} |\Phi_{M,k}(\beta, t)\rangle = H |\Phi_{M,k}(\beta, t)\rangle. \quad (19)$$

These differential equations can be solved by the use of straightforward iterator methods, e.g. Runge-Kutta⁸⁻¹⁰, or more sophisticated Chebyshev^{71,72} schemes. In this paper, we use a fourth order Runge-Kutta (RK4) scheme with a discrete time step $\delta t J = 0.01 \ll 1$. For this small δt , numerical errors are negligible, as shown later by the time-independent norm of $|\Phi_{M,k}(\beta, t)\rangle$ and $|\varphi_{M,k}(\beta, t)\rangle$ and the agreement with results from other methods.

In the Runge-Kutta scheme, we have to implement the action of Hamiltonian and currents on pure states. It is possible to carry out these matrix-vector multiplications without saving matrices in computer memory. Therefore, the memory requirement of the algorithm is set only by the size of vectors: $\mathcal{O}(d_{M,k})$. However, to reduce the run time of the algorithm, it is convenient to save matrices in memory. In this respect, we can profit from the fact that Hamiltonian and currents are few-body operators with a sparse-matrix representation, even in the common eigenbasis of symmetries. In fact, for all operators, there are only $L d_{M,k} \ll d_{M,k}^2$ nonvanishing matrix elements, as illustrated in Fig. 2 (a). Thus, the memory requirement of the algorithm is $\mathcal{O}(L d_{M,k})$ and scales linearly with the dimension of the symmetry subspaces. Consequently, we are able to treat chains with as many as $L = 33$ sites, where the largest subspaces at $M = 0$ are huge:

$$d_{0,k} \approx 3.5 \cdot 10^7. \quad (20)$$

As compared to the upper subspace dimension accessible to exact diagonalization, this dimension is orders of magnitude larger, i.e., by a factor $\mathcal{O}(10^4)$. Note that the dimension of the full Hilbert space is $d \approx 10^{10}$. In Fig. 2 (b) we show the run time of the algorithm for the largest subspaces and the spin current using a single CPU and 10^4 discrete time steps ($\delta t J = 0.01$, $t J = 100$). For $L = 33$, the run time is about one month while, for $L = 20$, the calculation takes about two minutes. We note that, for cases where less time steps are needed ($\delta t J = 0.01$, $t J \ll 100$), $L > 33$ calculations are also feasible within reasonable run time, as demonstrated in Sec. IV A.

Obviously, iterator methods for solving Eqs. (18) and (19) are very typical approaches to profit from massive parallelization. This has been pursued in other applications of typicality, *neglecting* however the impact of symmetry reduction⁷¹. Regarding our algorithm, the latter adds an additional layer of parallelization, i.e., due to the good quantum numbers (M, k) , each of the $(2L+1)L$ subspaces can be computed independently. Remarkably, in practice, we have only relied on the latter parallelization, using not more than L CPUs on medium-sized clusters. In this way, we were able to reach system sizes identical to those of massively parallelized codes on super computers without symmetry reduction^{71,72}. We believe that symmetry reduction in combination with massive parallelization has the potential to reach $L \sim 40$ in the future.

IV. SPIN-CURRENT DYNAMICS IN THE INTEGRABLE MODEL

First, we present results on the integrable model in Eq. (1). Since the energy current j_E is strictly conserved in this model, we focus on the dynamics of the spin current j_S . Parts of the corresponding results in Figs. 3, 4, and 5 have been shown in our previous work¹⁰. Subsequently,

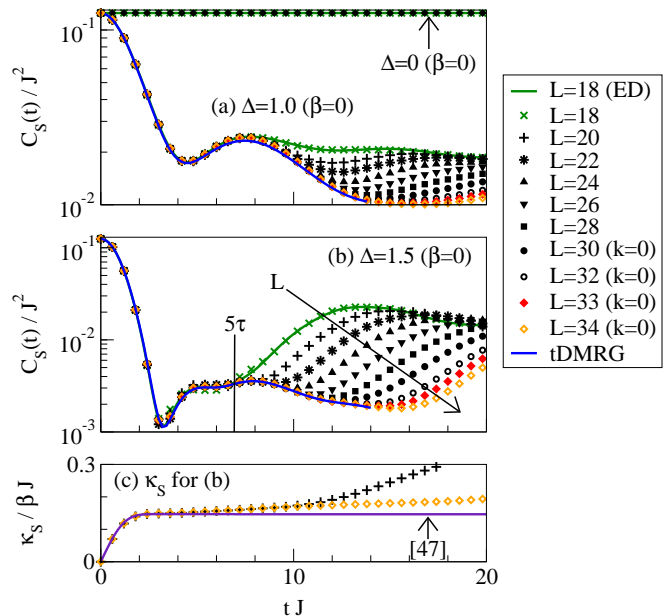


FIG. 3. (color online) Spin-current autocorrelation function $C_S(t)$ at $\beta \rightarrow 0$ for (a) $\Delta = 1.0$ and 0, (b) $\Delta = 1.5$, numerically obtained for $L = 18$ using the exact expression in Eq. (10) (green curve) and larger $L \geq 18$ using the approximation in Eq. (17) (symbols), shown in a semi-log plot. The very high accuracy of the approximation is illustrated by comparing to available tDMRG data for $L = 200$ ^{55,57} (blue curve). (c) Dc conductivity κ_S for (b), evaluated according to Eq. (11) as a function of the cutoff time. For comparison, the perturbative result of Ref. 47 is depicted (curve).

we also investigate the dynamics of the energy current for the nonintegrable model.

A. High Temperatures and Intermediate Times

We begin with the high-temperature limit $\beta \rightarrow 0$ and intermediate times $t J \leq 20$. For anisotropy $\Delta = 1$ and small $L = 18$, we compare in Fig. 3 (a) the exact and approximate expressions of the autocorrelation function in Eqs. (10) and (17), numerically calculated by the use of exact diagonalization and fourth order Runge-Kutta, respectively. For all times, the agreement between Eqs. (10) and (17) is remarkably good. Our usage of a semi-log plot underlines this agreement even more and emphasizes relative rather than only absolute accuracy. Due to this agreement, we can already consider the approximation as almost exact for $L = 18$. Moreover, any remaining error decreases exponentially fast with L . Thus, we can safely neglect any averaging over random pure states $|\psi\rangle$. Note that, for the models studied in this paper, significant errors only occur below $L \sim 10$, see Appendix D.

By increasing L in Fig. 3 (a), we show that the curve of the autocorrelation function gradually converges in time towards the thermodynamic limit. For the maximum size $L = 34$ calculated, the curve is converged up to times

$tJ \sim 15$ with no visible finite-size effects in the semi-log plot. For the four largest $L \geq 30$ depicted, we restrict ourselves to a single translation subspace, i.e., $k = 0$, to reduce computational effort in the high-temperature limit $\beta \rightarrow 0$. For these temperatures, it is already known that the k dependence is negligibly small³⁷, and we also do not observe a significant dependence on k for $L < 30$, see Appendix A.

Additionally, we compare to existing tDMRG data for a system of very large size $L = 200$ ⁵⁵. It is intriguing to see that our results agree up to very high precision. On the one hand, this very good agreement is a convincing demonstration of dynamical typicality in an integrable system. On the other hand, this agreement unveils that our numerical technique yields exact information on an extended time window in the thermodynamic limit $L \rightarrow \infty$. As shown later, this time window can become very large for nonintegrable systems.

In Fig. 3 (b) we show a second calculation for a larger anisotropy $\Delta = 1.5$. Clearly, the autocorrelation function decays to almost zero rapidly. However, there is a small long-time tail. This tail has been observed already on the basis of exact diagonalization for intermediate $L = 20$ ⁴⁶. It is not connected to the Drude weight⁵⁷, as discussed in more detail later. It is also not a finite-size effect, as evident from the agreement with tDMRG. While this tails shows the tendency to decay when comparing $tJ \sim 10$ and 15 , we relate its origin to the onset of revivals in the vicinity of the Ising limit⁵⁷. If we partially neglect the tail and determine the dc conductivity κ_S according to Eq. (11) for $t_3 J = 5\tau J = 7$, we get $\kappa_S/(\beta J) = 0.159$. This value agrees well with the theoretically predicted value 0.147 of the perturbation theory in Ref. 47, see Fig. 3 (c). Because this theory does not take into account the tail, both values slightly differ. For the maximum time without finite-size effects, $t_3 J = 10\tau J = 14$, we get $\kappa_S/(\beta J) = 0.178$. This value is still not larger than 20% of theoretical prediction, see also Ref. 57.

B. Long-Time Limit

Next, we investigate the long-time limit. In Fig. 4 (a) we show $C_S(t)$ in the high-temperature limit $\beta \rightarrow 0$ and various anisotropies $\Delta = 0.5, 1.0$, and 1.5 . Additionally, we depict the norm of $|\Phi_\beta(t)\rangle$. This norm is practically constant, as the norm of $|\varphi_\beta(t)\rangle$ also. The constant norm clearly demonstrates that the Runge-Kutta scheme works properly at such long times. The data in Fig. 4 (a) also proves the saturation of $C_S(t)$ at rather long time scales $tJ \sim 50$. Furthermore, we can hardly infer the saturation value from our short-time data in Fig. 3. We note that no fluctuations are visible in the long-time limit since the approximation error of our numerical approach is exponentially small and practically zero for the large system sizes depicted.

In contrast to short times, the long-time limit is still governed by finite-size effects. Hence, we are now go-

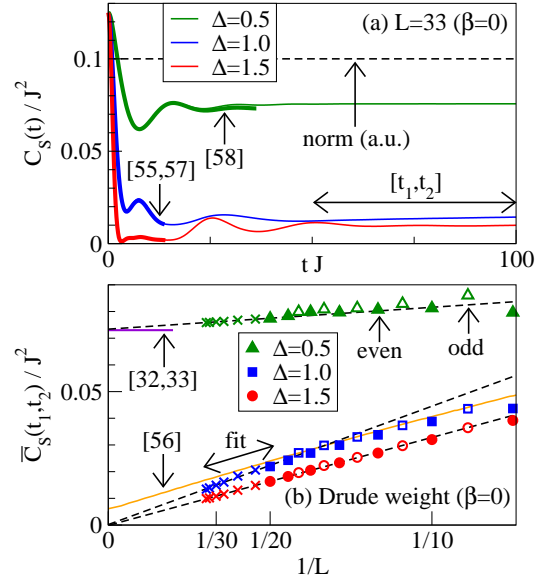


FIG. 4. (color online) (a) Long-time limit of the spin-current autocorrelation function $C_S(t)$ at $\beta \rightarrow 0$ for $\Delta = 0.5, 1.0$, and 1.5 , numerically obtained using the approximation in Eq. (17) (thin solid curves). The well-conserved norm is indicated (thin dashed curve). Available tDMRG data for $L = 200$ ^{55,57,58} is depicted (thick solid curves). (b) Finite-size scaling of the spin Drude weight, extracted according to Eq. (11) in the time interval $[t_1 J, t_2 J] = [50, 100]$ (small $L \leq 20$: exact expression in Eq. (10), closed (open) symbols for even (odd) L ; large $L > 20$: approximation in Eq. (17), crosses). Simple $1/L$ fits to large $20 \leq L \leq 33$ are shown (dashed lines), and at $\Delta = 1.0$ the odd-site fit to $L \leq 19$ performed in Ref. 56 as well (solid curve). At small $\Delta = 0.5$, T. Prosen's rigorous analytic lower bound^{32,33} is indicated (horizontal line).

ing to perform a proper finite-size scaling for the Drude weight. We use the definition of the Drude weight according to Eq. (11) and average over the time interval $[t_1 J, t_2 J] = [50, 100]$, without invoking assumptions. The Drude weight has been extracted the same way in Ref. 46. Moreover, this way of extracting the Drude weight reproduces the correct zero-frequency values for small L in, e.g., Ref. 35.

In Fig. 4 (b) we depict the resulting Drude weight vs. the inverse length $1/L$ for anisotropies $\Delta = 0.5, 1.0$, and 1.5 . For $L > 20$, we extract the Drude weight from the approximation in Eq. (17) (denoted by crosses) and, for $L \leq 20$, we use the exact expression in Eq. (10) (denoted by other symbols). In this way, we avoid typicality errors at small L . We also indicate the results of $1/L$ fits, solely based on data points for $L \geq 20$. In this way, we avoid the need of $(1/L)^{i>1}$ corrections as well as the influence of even-odd effects at small L and, especially, at small Δ ⁷⁶, see Fig. 4 (b). For the small $\Delta = 0.5$, the resulting fit is close to all data points. Furthermore, extracting the thermodynamic limit $L \rightarrow \infty$ from the fit, we find a non-zero Drude weight in convincing agreement with the rigorous lower bound of Refs. 32 and 33. While the situ-

ation is rather similar for the large anisotropy $\Delta = 1.5$, the Drude weight vanishes, in agreement with previous work³⁵. The isotropic point $\Delta = 1.0$ is certainly the most interesting case. Here, the $L \geq 20$ fit is not close to the one obtained from only small $L < 20$. In fact, the extrapolation yields much smaller values for the Drude weight than the finite values suggested in previous works, based on either smaller L ^{35,56} or shorter t ⁵⁵ (see also Ref. 56 for a comprehensive discussion). Moreover, our result points to a vanishing Drude weight for $L \rightarrow \infty$.

In Fig. 5 we summarize the finite-size values for the Drude weight for fixed $L = 30$ and various anisotropies $0 \leq \Delta \leq 1.5$. Additionally, we indicate the extrapolated values for $L \rightarrow \infty$ using fits. Since even-odd effects are stronger closer to the point $\Delta = 0$, we take into account only even sites for the fits. Remarkably, all extrapolated values lie above the rigorous lower bound of Refs. 32 and 33, and in the anisotropy range $0.4 \lesssim \Delta \leq 1.5$, also agree with the Bethe-Ansatz solution of Ref. 30. They further agree with an alternative extrapolation on the basis of small L ³⁷, using a different statistical ensemble and only odd sites. In the vicinity of the point $\Delta = 0$, we still lie above the lower bound but we observe deviations from the Bethe-Ansatz result. These deviations do *not* indicate the breakdown of typicality and are well-known to occur in numerical studies using finite systems³⁷, due to the very high degeneracy at $\Delta = 0$. As visible in Fig. 5, tDMRG results for $\Delta \sim 0.3$ also show these deviations and are in very good agreement with our results.

C. Low Temperatures

We now turn to finite temperatures $\beta \neq 0$. Clearly, the approximation in Eq. (17) has to break down for $\beta \rightarrow \infty$, i.e., $T \rightarrow 0$, due to the reduction of the effective Hilbert space dimension d_{eff} . Recall that d_{eff} essentially counts the number of thermally occupied states. Furthermore,

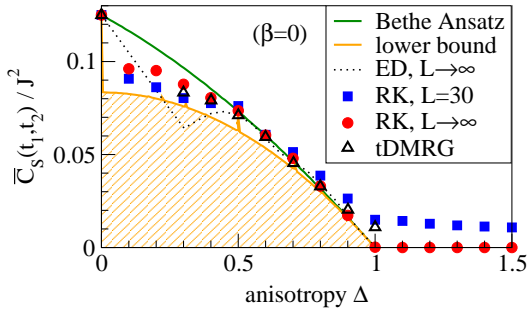


FIG. 5. (color online) High-temperature spin Drude weight \bar{C}_S w.r.t. the anisotropy Δ , obtained from the approximation in Eq. (17) using Runge-Kutta (closed symbols). Results are compared to the thermodynamic Bethe Ansatz³⁰, T. Prosen's strict analytic lower bound^{32,33}, the extrapolation based on exact diagonalization at zero magnetization and odd sites in Ref. 37, and tDMRG⁵⁵ (see also Ref. 56 for a different point of view on the tDMRG data point at $\Delta = 1$).

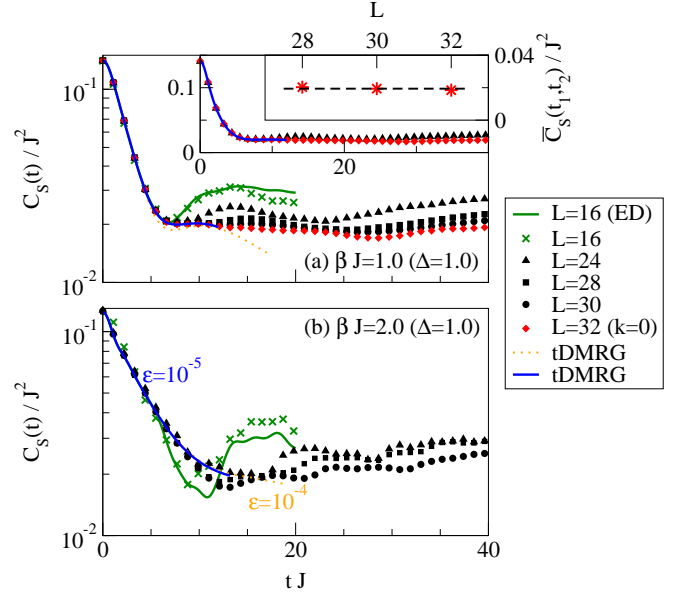


FIG. 6. (color online) Spin-current autocorrelation function $C_S(t)$ for the isotropic point $\Delta = 1.0$ at (a) $\beta J = 1.0$ and (b) $\beta J = 2.0$, numerically obtained for $L = 16$ using the exact expression in Eq. (10) (green curve) and larger $L \geq 16$ using the approximation in Eq. (17) (symbols), shown in a semi-log plot. Available tDMRG data for $L = 200$ ^{55,56} is depicted for two different values of the discarded weight ϵ (blue and orange curve). Inset in (a): lin-lin plot of (a) for $L = 24$ and 32 ; and inset therein: average height $\bar{C}(t_1, t_2)$ of the plateau at times $[t_1 J, t_2 J] = [10, 40]$ for the three largest L where this plateau is clearly seen. The horizontal line is a guide to the eye.

for $\beta J \gg 2$, also the exact expression in Eq. (10) is governed by large finite-size effects, at least for a finite system of size $L \sim 30$ ⁴⁸. Thus, for a numerical approach to $L \sim 30$, reasonable temperatures are $\beta J \sim 2$. For this range of β , the approximation is still justified and averaging over pure states is necessary for $\beta \gg 2$ only. This temperature, however, depends on the specific model, as discussed later in more detail for the nonintegrable system.

For a small size $L = 16$, anisotropy $\Delta = 1$, and the two lower temperatures $\beta J = 1$ and 2 , we compare in Figs. 6 (a) and (b) the exact expression in Eq. (10) and the approximation in Eq. (17), calculated by the use of exact diagonalization and Runge-Kutta, respectively. Clearly, deviations appear at $\beta J = 2$. However, these deviations manifest as random fluctuations rather than systematic drifts and may be compensated by additional averaging over several pure states $|\psi\rangle$. Furthermore, one can expect that these deviations disappear for significantly larger sizes L . Again, we prove this expectation by comparing with available tDMRG data for $L = 200$ ^{55,56}. The very good agreement illustrates the power of our numerical approach at finite temperatures. Moreover, taking into account the simple structure of the curve, the semi-log plot, and the combination of tDMRG with our numerical approach, Fig. 6 (a) points to non-zero Drude weights at

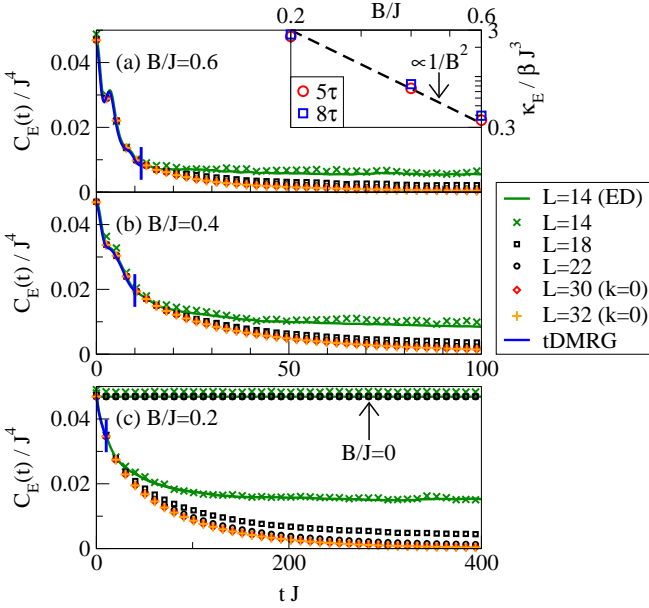


FIG. 7. (color online) Real-time decay of the energy-current autocorrelation function $C_E(t)$ for the XXZ spin-1/2 chain at anisotropy $\Delta = 0.5$ in a staggered magnetic field of strength (a) $B/J = 0.6$, (b) $B/J = 0.4$, and (c) $B/J = 0.2$ in the high-temperature limit $\beta J \rightarrow 0$. Numerical results according to Eq. (17) for length $L = 14$ agree well with both, exact diagonalization and available tDMRG data for $L = 200$ in Ref. 60. (The maximum time of this tDMRG data is indicated by vertical blue bars.) For $L > 14$, little finite-size effects are visible up to full relaxation, e.g., $L = 22$ and $L = 32$ are indistinguishable in (a)-(c). Inset in (a): The dc conductivity κ_E according to Eq. (11) with $t_3 = 5\tau$ and 8τ scales $\propto 1/B^2$ for small values of B .

$\beta \neq 0$. This observation is different from our previous results at $\beta = 0$. Still there are finite-size effects for the three largest values of L where a plateau is clearly seen at times $[t_1 J, t_2 J] = [10, 40]$. But these finite-size effects are hardly visible in a lin-lin plot, see the inset in Fig. 6 (a). Moreover, extrapolations are impossible on the basis of three and approximately constant points, see the inset therein.

It is further worth mentioning that the possibility of non-vanishing Drude weights at $\beta \neq 0$ is consistent with the recent upper bound in Ref. 75. This upper bound does *not* vanish when taking into account all sectors of magnetization, as done in our paper.

V. ENERGY-CURRENT DYNAMICS IN THE NONINTEGRABLE MODEL

Next, we extend our analysis in two directions. First, we break the integrability of the model by the staggered magnetic field in Eq. (7). Second, we expand our analysis to include the dynamics of the energy current j_E , which is *not* conserved anymore in the nonintegrable model.

A. Dependence on Magnetic Field and Anisotropy

Again, we begin with the high-temperature limit $\beta \rightarrow 0$ and compare the exact expression in Eq. (10), evaluated by exact diagonalization, and the approximation in Eq. (17), evaluated by Runge-Kutta, for the energy current j_E . We show this comparison in Figs. 7 (a)-(c) for a small size $L = 14$, anisotropy $\Delta = 0.5$, and magnetic fields of different strength $B/J = 0.6, 0.4$, and 0.2 . Apparently, Eqs. (10) and (17) agree well with each other. This good agreement proves that dynamical typicality is neither a particular property of the spin current j_s nor restricted to the integrable system. Interestingly, our $L = 14$ data already reproduces existing tDMRG data for $L = 200$ in Ref. 60. We note that exact-diagonalization data for $L = 12$ does so also, although not shown here explicitly.

For small $L = 14$ and all $B/J \neq 0$ in Fig. 7 (a)-(c), the energy-current autocorrelation function $C_E(t)$ does not decay to zero and features a nonzero Drude weight. The actual value of the finite-size Drude weight increases as B is decreased. However, by increasing L , we show that $C_E(t)$ decays to zero for significantly larger L and all B considered. Moreover, we find that $C_E(t)$ is practically the same for $L = 22$ and $L = 32$. This finding indicates little finite-size effects up to full relaxation. Hence, our numerical approach yields exact information on the full, physically relevant time window in the thermodynamic limit $L \rightarrow \infty$.

Let us discuss the relaxation curve for large L in more detail. The relaxation time decreases as B increases and the overall structure of the curve is simple, in particular without any slowly decaying long-time tails. Therefore, extracting from our numerical data the dc conductivity κ_E according to Eq. (11) yields similar values for cutoff times $t_3 = 5\tau$ and 8τ . These values are shown in the inset of Fig. 7 (a). The apparent decrease of κ_E with B results from the decrease of τ with B and our usage of a log-

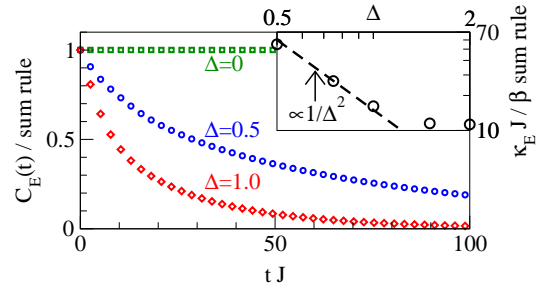


FIG. 8. (color online) Real-time decay of the energy-current autocorrelation function $C_E(t)$ for the XXZ spin-1/2 chain at various anisotropies $\Delta = 0, 0.5$, and 1 in a staggered magnetic field of strength $B/J = 0.2$ in the high-temperature limit $\beta J \rightarrow 0$. All initial values are normalized to 1, i.e., divided by the sum rule $J^4(1 + 2\Delta^2)/32$. Inset: In units of the sum rule, the dc conductivity according to Eq. (11) scales $\propto 1/\Delta^2$ for small values of Δ . The system size is $L = 30$ ($k = 0$) in all cases.

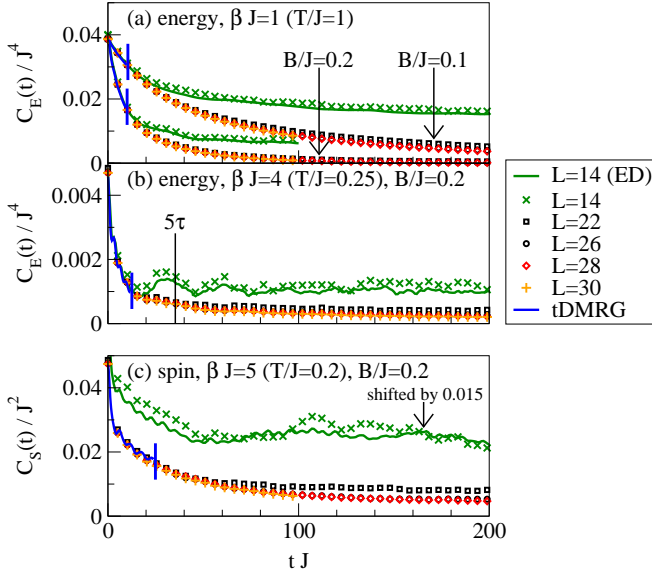


FIG. 9. (color online) Real-time decay of the autocorrelation functions of (a), (b) energy current and (c) spin current for the Heisenberg spin-1/2 chain at anisotropy $\Delta = -0.85$ in a staggered magnetic field of strength $B/J \leq 0.2$. Numerical results according to Eq. (17) for length $L = 14, \dots, 30$ agree well with available tDMRG data in Ref. 59 and show little finite-size effects over the temperature range $\beta J \leq 5$ ($T/J \geq 0.2$). In (c) $L = 14$ data is shifted by 0.015 since this data is very close to $L > 14$ data.

log plot unveils the scaling $\kappa_E \propto 1/B^2$, as expected from conventional perturbation theory at small B ^{67,68}. Note that the commutator in Eq. (8) essentially is the memory kernel of the perturbation theory and yields scattering rates $1/\tau \propto (B\Delta)^2/(1+2\Delta^2)$ and hence, in units of the sum rule, the scaling

$$\kappa'_E = \frac{\kappa_E}{1+2\Delta^2} \propto \frac{1+2\Delta^2}{(B\Delta)^2}, \quad (21)$$

i.e., $\kappa_E = \kappa'_E \propto 1/(B\Delta)^2$ for small values of Δ . A more detailed description of the perturbation theory is given in Appendix B.

To verify the Δ dependence from perturbation theory, we calculate in Fig. 8 the energy-current autocorrelation function $C_E(t)$ for different $\Delta = 0, 0.5$ and 1 , at fixed magnetic field $B/J = 0.2$ and size $L = 30$. Indeed, $C_E(t)$ decays the slower the smaller Δ and no dynamics occurs at $\Delta = 0$. Moreover, extracting the dc conductivity κ'_E from our numerical data, we find the scaling $\kappa'_E \propto 1/\Delta^2$ at small Δ , as shown in the inset of Fig. 8. This scaling turns into $\kappa'_E = \text{const.}$ at large Δ , still consistent with the expectation from perturbation theory.

B. Temperature Dependence

We now turn to finite temperatures $\beta \neq 0$ and choose the parameters of the model according to the availability

of tDMRG data in the literature. Such data is available for negative anisotropy $\Delta = -0.85$ ⁵⁹, where the model is still antiferromagnetic. We note that the sign of Δ has not been of importance so far since, at high temperatures $\beta \rightarrow 0$, the dynamics depends on $|\Delta|$ only.

In Figs. 9 (a) and (b) we summarize our results on the energy-current autocorrelation function $C_E(t)$ for an intermediate temperature $\beta J = 1$ and a low temperature $\beta J = 4$. Moreover, we depict our results on the spin-current autocorrelation function $C_S(t)$ for an even lower temperature of $\beta J = 5$ in Fig. 9 (c). While the focus is on a magnetic field of strength $B/J = 0.2$, Fig. 9 (a) also shows results for the case $B/J = 0.1$. Several comments are in order. First, already for a small system size of $L = 14$, the exact expression in Eq. (10) and the approximation in Eq. (17) are in good agreement at $\beta J = 1$. While deviations occur at $\beta \gg 1$, these deviations are surprisingly small for both, the energy and spin current in Figs. 9 (b) and (c). Second, our exact-diagonalization data for $L = 14$ already reproduces existing tDMRG data for $L = 200$ in Ref. 59 for the whole temperature range $\beta J \leq 5$. This observation is indeed interesting, especially since lower temperatures have not been analyzed by tDMRG⁵⁹, at least for the energy current. Third, our results for large L do not depend significantly on L . This independence demonstrates the high accuracy of the approximation in Eq. (17) for large L and also indicates little (or weakly scaling) finite-size effects.

Because we do not need to deal with finite-size effects, we may directly extract from our numerical data the dc conductivity κ_E in Eq. (11), starting with the cutoff time $t_3 = 5\tau$. This choice has been sufficient for high temperatures and its role for low temperatures is discussed later in detail. For the energy current and another negative anisotropy $\Delta = -0.95$, we show in Fig. 10 the resulting

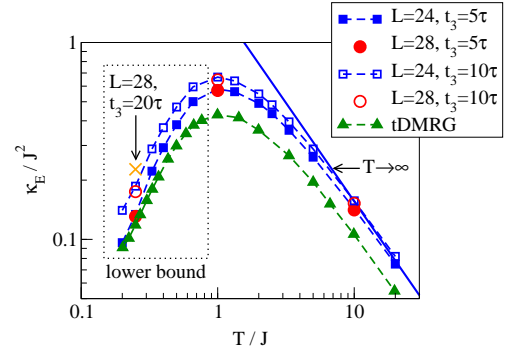


FIG. 10. (color online) T dependence of the dc conductivity κ_E for the XXZ spin-1/2 chain at anisotropy $\Delta = -0.95$ in a staggered magnetic field of strength $B/J = 0.2$, calculated according to Eq. (11) for $t_3 = 5\tau$ and 10τ . For comparison, results from tDMRG-based fits/extrapolations in Ref. 59 are shown. While the overall agreement is quite good, deviations are clearly visible and neither a finite-size effect nor an effect arising from the specific choice of t_3 . The dotted box indicates the T region where our results on κ_E have to be understood as an lower bound.

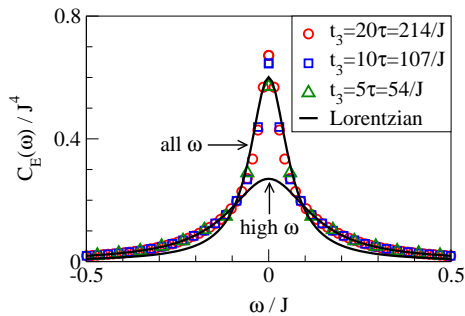


FIG. 11. (color online) Fourier-transformed energy-current autocorrelation function $C_E(\omega)$ for the Heisenberg spin-1/2 chain at anisotropy $\Delta = -0.95$ in a staggered magnetic field of strength $B/J \leq 0.2$ at temperature $\beta J = 1$. The Fourier transform is performed over time intervals $t_3 = 5\tau$, 10τ , and 20τ for a system of size $L = 28$. The results of Lorentzian fits to $C_E(\omega)$ at all ω and $|\omega|/J \geq 0.1$ are indicated.

temperature dependence of κ_E in a log-log plot. Apparently, $\kappa_E \propto \beta = 1/T$ in the limit of high temperatures $T/J \gg 1$. This scaling with T is a direct consequence of the trivial prefactor β in Eq. (11) and shows that the actual energy-current autocorrelation $C_E(t)$ turns T independent in that limit. At $T/J \sim 1$, the high-temperature limit is clearly left and $\kappa_E(T)$ features a broad maximum. At $T/J \ll 1$, the low-temperature regime sets in and the scaling of κ_E with T is consistent with a power law, however, the exponent remains an open issue. Remarkably, this power-law scaling mainly results from the initial value $C_E(0)$ and not from the time dependence $C_E(t)$ as such, cf. Figs. 9 (a) and (b).

In Fig. 10 we additionally compare these results on $\kappa_E(T)$ with results from tDMRG. Precisely, we compare to results from fits/extrapolations performed in Ref. 59 on the basis of short-time tDMRG data, cf. Figs. 9 (a) and (b). While the overall agreement is quite good, our $\kappa_E(T)$ lies above the one of Ref. 59 for all temperatures $0.2 \leq T/J \leq 20$. We emphasize that this deviation is not a finite-size effect and, moreover, that it does not result from our choice $t_3 = 5\tau$ for the calculation of κ_E . In fact, using a longer time $t_3 = 10\tau$ yields a positive correction to κ_E and hence increases the deviation, as illustrated in Fig. 10. This correction is again small at high temperatures: At $T/J = 10$, the correction is only 8% and, at $T/J = 1$, the correction is slightly higher with 13%. But the trend indicates that $C_E(t)$ exhibits slowly decaying long-time tails at low temperatures. Furthermore, such a tail is clearly visible at $T/J = 0.25$ in Fig. 9 (b). For this low temperature, our choice of $t_3 = 5\tau$ or 10τ seems to underestimate κ_E significantly and has to be understood as a *lower bound*. We explicitly avoid analyzing longer t_3 since we cannot exclude the possibility of (weakly scaling) finite-size effects in the long-time limit.

To gain further insight and to provide an alternative point of view, we show in Fig. 11 the Fourier-transformed energy-current autocorrelation function $C_E(\omega)$, still for anisotropy $\Delta = 0.95$ and magnetic field $B/J = 0.2$, at

temperature $\beta J = 1$. This parameter set corresponds to the maximum visible in Fig. 10. The Fourier transform is performed for different $t_3 = 5\tau$, 10τ , and 20τ . Note that the longest time is $20\tau = 214/J$. While $C_E(\omega)$ at $|\omega|/J \geq 0.1$ does not depend on the specific choice of t_3 , it does at $|\omega|/J \ll 0.1$. Clearly, a minimum time $\sim 10\tau$ is required to determine the limit $\omega \rightarrow 0$ with sufficient accuracy, as a consequence of slowly decaying long-time tails at low temperatures. We also indicate the result of a Lorentzian fit to $C_E(\omega)$ at $|\omega|/J \geq 0.1$. Evidently, this high-frequency/short-time fit cannot be used to predict the dc value correctly. This fact illustrates the origin of the underestimation in Ref. 59. We stress that the overall form of $C_E(\omega)$ is not Lorentzian at all, while our previous results in the limit of high temperatures agree well with a Lorentzian line shape, see Appendix C.

VI. SUMMARY

In summary, we used the concept of typicality to study the real-time relaxation of spin and energy currents in spin-1/2 chains at finite temperatures. These chains were the integrable XXZ chain and a nonintegrable version due to the presence of a staggered magnetic field oriented in z direction. In the framework of linear response theory, we numerically calculated autocorrelation functions by propagating a single pure state, drawn at random as a typical representative of the full statistical ensemble. By comparing to data from exact diagonalization for small system sizes and existing data from tDMRG for short times, we showed that typicality holds in finite systems over a wide range of temperature and is fulfilled in both, integrable and nonintegrable systems.

For the integrable model, we calculated the dynamics of the spin current for long times and extracted the spin Drude weight for large system sizes outside the range of state-of-the-art exact diagonalization. Employing proper finite-size scaling, we provided strong evidence that, at high temperatures above the exchange coupling constant J , the Drude weight vanishes at the isotropic point. This finding, and also our results for other values of the exchange anisotropy, were in good agreement with existing Bethe-Ansatz and Mazur-inequality results. For lower temperatures on the order of J , we found at least indications that the Drude weight is nonzero at the isotropic point.

For the nonintegrable model, we calculated the decay of the energy current for large system sizes and did not observe significant finite-size effects. Therefore, we were able to obtain the full decay curve in the thermodynamic limit and to extract the dc conductivity without invoking difficult fits/extrapolations. Analyzing the dependence of the dc conductivity on the parameters of the model, we found a quadratic scaling with the inverse magnetic field and exchange anisotropy, in agreement with conventional perturbation theory. Moreover, we detailed the temperature dependence of the dc conductivity, including low-

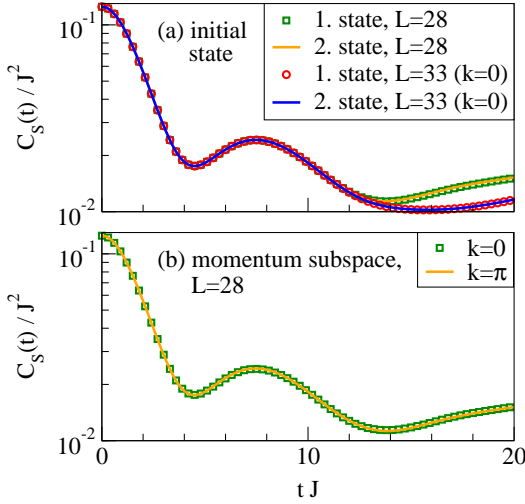


FIG. 12. (color online) Spin-current autocorrelation function $C_S(t)$ in the integrable model at anisotropy $\Delta = 1.0$ and high temperatures $\beta \rightarrow 0$ for (a) two different initial states and (b) two different momentum subspaces, numerically obtained for $L = 28$ and 33 using the approximation in Eq. (17).

and high-temperature power laws with an intermediate maximum. Our numerical results seem to provide a lower bound on the dc conductivity.

From a merely numerical point of view, we profit from two central advantages of the typicality-based technique used in this paper. First, the numerical technique allows us to perform finite-size scaling. This is certainly similar to exact diagonalization. However, system sizes are much larger and extrapolations are more reliable. Second, the numerical technique also yields exact information on an extended time window in the thermodynamic limit. This is certainly similar to tDMRG. However, time windows accessible seem to be much longer for generic nonintegrable systems, as evident for the example studied in this paper. Because of these two advantages, our numerical method may complement other numerical approaches in a much broader context, including problems with few symmetries and/or in two dimensions. Moreover, our numerical method may be applied to other observables⁸ and not only to current operators.

ACKNOWLEDGMENTS

We sincerely thank H. Niemeyer, P. Prelovšek, and J. Herbrych for fruitful discussions as well as C. Karrasch and F. Heidrich-Meisner for the tDMRG data in Sec. IV (Refs. 55–58) and helpful comments. The tDMRG data in Sec. V (Refs. 59 and 60) have been digitized.

Part of this work has been done at the Platform for Superconductivity and Magnetism, Dresden. Part of this work has been supported by DFG FOR912 Grant No. BR 1084/6-2, by SFB 1143, as well as by EU MC-ITN LOTHERM Grant No. PITN-GA-2009-238475.

Appendix A: Independence of the Specific Initial State and Momentum Subspace

In Fig. 12 we demonstrate that for large system sizes L the approximation in Eq. (17) depends neither on the specific realization of the random initial state $|\psi\rangle$ nor on the momentum subspace k considered. Because both facts are particularly relevant for the finite-size scaling of the spin Drude weight in Fig. 4, we present in Fig. 12 results for the integrable model in Eq. (1) at anisotropy $\Delta = 1$ in the limit of high temperatures $\beta \rightarrow 0$. In this limit, the independence of initial states and momentum subspace holds for all examples given in this paper. For low temperatures, we explicitly avoid the restriction to a single momentum subspace since the independence of k is not ensured in this temperature regime, also for the exact expression in Eq. (10).

Appendix B: Perturbation Theory for the Energy Current

We discuss here the perturbation theory for the energy current in detail. Since the energy current j_E is strictly conserved for the integrable Hamiltonian H , $[j_E, H] = 0$, the staggered Zeeman term H_B can be identified as the only origin of scattering. This scattering can be treated perturbatively according to Refs. 67–70 if the strength of the magnetic field B is a sufficiently small parameter. In the time domain, we can formulate such a perturbation theory in terms of the integro-differential equation

$$\dot{C}_E(t) = - \int_0^t dt' K(t-t') C_E(t'), \quad (\text{B1})$$

where $K(t)$ is the memory kernel. To lowest order of B , B^2 , this memory kernel reads in the high-temperature

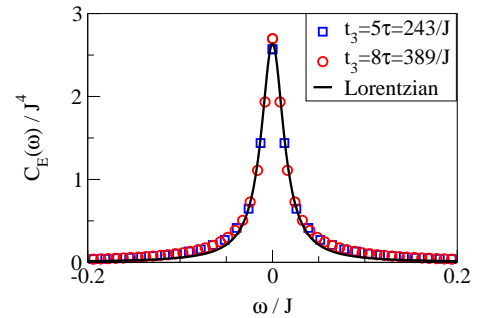


FIG. 13. (color online) Fourier-transformed energy-current autocorrelation function $C_E(\omega)$ for the XXZ spin-1/2 chain at anisotropy $\Delta = 0.5$ in a staggered magnetic field of strength $B/J \leq 0.2$ in the high-temperature limit $\beta \rightarrow 0$. The Fourier transform is performed over time intervals $t_3 = 5\tau$ and 8τ for system size $L = 32$ ($k = 0$). The result of a Lorentzian fit to $C_E(\omega)$ at all ω is indicated.

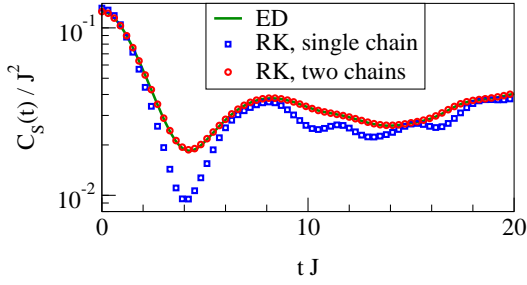


FIG. 14. (color online) Spin-current autocorrelation function $C_S(t)$ in the integrable model at anisotropy $\Delta = 1.0$ and high temperatures $\beta \rightarrow 0$, numerically obtained for a small system size $L = 10$ using different methods: (i) exact diagonalization, the approximation in Eq. (17) for a (ii) single chain and (iii) two identical, uncoupled chains.

limit $\beta \rightarrow 0$ ^{67,68}

$$K(t) = \frac{\text{Tr}\{\iota[J_E, H_B]_I(t) \iota[J_E, H_B]\}}{\text{Tr}\{J_E^2\}} \propto \frac{(B\Delta)^2}{1 + 2\Delta^2}, \quad (\text{B2})$$

where the subscript I of the first commutator indicates the interaction picture w.r.t. H . Despite the integrability of H , exactly calculating the time dependence of $K(t)$ is very difficult and requires, e.g., the exact diagonalization of a finite system^{69,70}. For our purposes, however, it is sufficient to use the well-known Markov approximation $K(t) = K\delta(t)$. This approximation is reasonable in the limit of small magnetic fields $B \rightarrow 0$, where relaxation is arbitrarily slow. In this way, we obtain from Eq. (B1) the exponential relaxation

$$\frac{C_E(t)}{C_E(0)} = e^{-Kt}, \quad C_E(0) = \frac{1 + 2\Delta^2}{32} \quad (\text{B3})$$

corresponding to a Lorentzian line shape in frequency space. Thus, using the expression for the dc conductivity κ_E in Eq. (11) with $t_3 \rightarrow \infty$, we find the scaling

$$\kappa'_E = \frac{\kappa_E}{1 + 2\Delta^2} \propto \frac{1 + 2\Delta^2}{(B\Delta)^2}. \quad (\text{B4})$$

The quantity κ'_E introduced does not include a trivial scaling due to the sum rule $C_E(0)$ and is the prediction of the perturbation theory as such. For small values of Δ , we eventually find the scaling $\kappa_E = \kappa'_E \propto 1/(B\Delta)^2$ and, for large values of Δ , we find κ'_E to be independent of Δ . In this case, $\kappa_E \propto (\Delta/B)^2$.

Appendix C: Fourier Transform at High Temperatures

In Fig. 13 we show that the Fourier transform of our numerical results for the time-dependent energy-current autocorrelation function $C_E(t)$ at high temperatures, i.e. $\beta \rightarrow 0$, yields a Lorentzian line shape of $C_E(\omega)$ in frequency space. This line shape is another convincing indicator for the validity of conventional perturbation theory.

Appendix D: Typicality in Small Systems

Throughout this paper we have provided a comparison with exact-diagonalization data to prove that typicality already holds in finite systems of intermediate size, i.e., $L = 14 - 18$. It is clear that typicality has to break down for small systems. For the models studied in this paper, we observe this breakdown for sizes below $L \sim 10$, i.e., for effective dimensions below $d_{\text{eff}} \sim 1000$. In Fig. 14 we show one representative example.

However, a simple idea also allows us to use typicality for small L : Consider two identical, uncoupled chains of length L with the Hamiltonian

$$H' = H \otimes 1 + 1 \otimes H \quad (\text{D1})$$

and the current $j' = j \otimes 1 + 1 \otimes j$, respectively. In this way, we do not change the exact current dynamics but increase the dimension of the Hilbert space by a factor of 2^L . For the enlarged space, we can expect that typicality holds again. Figure 14 verifies this expectation.

We emphasize that the preceding is equivalent to *averaging*. The random state $|\psi\rangle$ from the $2^L \cdot 2^L$ dimensional Hilbert space has a Schmidt decomposition

$$|\psi\rangle = \sum_{i=1}^{2^L} a_i |u_i\rangle \otimes |v_i\rangle, \quad (\text{D2})$$

where a_i are random coefficients and $|u_i\rangle, |v_i\rangle$ are random orthonormal basis sets for each of the 2^L dimensional subspaces. Therefore, using a single random state in the doubled system is equivalent to a randomly weighted average over $2 \cdot 2^L$ autocorrelations functions, each calculated using one of $2 \cdot 2^L$ randomly chosen states. If this is more efficient than full diagonalization will depend on details.

We note that one can analogously consider more than two chains and therefore use typicality for any smaller L .

* r.steinigeweg@tu-bs.de

† jgemmer@uos.de

‡ w.brenig@tu-bs.de

¹ J. Gemmer and G. Mahler, Eur. Phys. J. B **31**, 249 (2003).

² S. Goldstein *et al.*, Phys. Rev. Lett. **96**, 050403 (2006).

³ S. Popescu, A. J. Short, and A. Winter, Nature Phys. **2**,

754 (2006).

⁴ P. Reimann, Phys. Rev. Lett. **99**, 160404 (2007).

⁵ S. R. White, Phys. Rev. Lett. **102**, 190601 (2009).

⁶ S. Sugiura and A. Shimizu, Phys. Rev. Lett. **108**, 240401 (2012).

⁷ C. Bartsch and J. Gemmer, Phys. Rev. Lett. **102**, 110403

- (2009); EPL **96**, 60008 (2011).
- ⁸ T. A. Elsayed and B. V. Fine, Phys. Rev. Lett. **110**, 070404 (2013).
 - ⁹ R. Steinigeweg *et al.*, Phys. Rev. Lett. **112**, 130403 (2014).
 - ¹⁰ R. Steinigeweg, J. Gemmer, and W. Brenig, Phys. Rev. Lett. **112**, 120601 (2014).
 - ¹¹ A. Hams and H. De Raedt, Phys. Rev. E **62**, 4365 (2000).
 - ¹² J. M. Deutsch, Phys. Rev. A **43**, 2046 (1991).
 - ¹³ M. Srednicki, Phys. Rev. E **50**, 888 (1994).
 - ¹⁴ M. Rigol, V. Dunjko, and M. Olshanii, Nature **452**, 854 (2008).
 - ¹⁵ M. A. Cazalilla and M. Rigol, New J. Phys. **12**, 055006 (2010); and references therein.
 - ¹⁶ I. Appelbaum, B. Huang, and D. J. Monsma, Nature **447**, 295 (2007).
 - ¹⁷ N. Tombros *et al.*, Nature **448**, 571 (2007).
 - ¹⁸ N. P. Stern *et al.*, Nature Phys. **4**, 843 (2008).
 - ¹⁹ F. Kuemmeth *et al.*, Nature **452**, 448 (2008).
 - ²⁰ A. V. Sologubenko *et al.*, Phys. Rev. Lett. **84**, 2714 (2000).
 - ²¹ C. Hess *et al.*, Phys. Rev. B **64**, 184305 (2001).
 - ²² N. Hlubek *et al.*, Phys. Rev. B **81**, 20405R (2010).
 - ²³ K. R. Thurber *et al.*, Phys. Rev. Lett. **87**, 247202 (2001).
 - ²⁴ H. Kühne *et al.*, Phys. Rev. B **80**, 045110 (2009).
 - ²⁵ H. Maeter *et al.*, J. Phys.: Condens. Matter **25**, 365601 (2013).
 - ²⁶ F. Xiao *et al.*, arXiv:1406.3202 (2014).
 - ²⁷ X. Zotos, F. Naef, and Prelovšek, Phys. Rev. B **55**, 11029 (1997).
 - ²⁸ A. Klümper and K. Sakai, J. Phys. A **35**, 2173 (2002).
 - ²⁹ B. S. Shastry and B. Sutherland, Phys. Rev. Lett. **65**, 243 (1990).
 - ³⁰ X. Zotos, Phys. Rev. Lett. **82**, 1764 (1999).
 - ³¹ J. Benz *et al.*, J. Phys. Soc. Jpn. **74**, 181 (2005).
 - ³² T. Prosen, Phys. Rev. Lett. **106**, 217206 (2011).
 - ³³ T. Prosen and E. Ilievski, Phys. Rev. Lett. **111**, 057203 (2013).
 - ³⁴ B. N. Narozhny, A. J. Millis, and N. Andrei, Phys. Rev. B **58**, 2921R (1998).
 - ³⁵ F. Heidrich-Meisner *et al.*, Phys. Rev. B **68**, 134436 (2003).
 - ³⁶ F. Heidrich-Meisner, A. Honecker, and W. Brenig, Eur. Phys. J. Special Topics **151**, 135 (2007).
 - ³⁷ J. Herbrych, P. Prelovšek, and X. Zotos, Phys. Rev. B **84**, 155125 (2011).
 - ³⁸ R. Steinigeweg, J. Herbrych, and P. Prelovšek, Phys. Rev. E **87**, 012118 (2013).
 - ³⁹ S. Fujimoto and N. Kawakami, Phys. Rev. Lett. **90**, 197202 (2003).
 - ⁴⁰ D. C. Johnston *et al.*, Phys. Rev. B **61**, 9558 (2000).
 - ⁴¹ S. Trotzky *et al.*, Science **319**, 295 (2007).
 - ⁴² P. Gambardella, Nature Mat. **5**, 431 (2006).
 - ⁴³ M. Kruczenski, Phys. Rev. Lett. **93**, 161602 (2004).
 - ⁴⁴ Y. B. Kim, Phys. Rev. B **53**, 16420 (1996).
 - ⁴⁵ K. Fabricius and B. M. McCoy, Phys. Rev. B **57**, 8340 (1998).
 - ⁴⁶ R. Steinigeweg and J. Gemmer, Phys. Rev. B **80**, 184402 (2009).
 - ⁴⁷ R. Steinigeweg and W. Brenig, Phys. Rev. Lett. **107**, 250602 (2011).
 - ⁴⁸ A recent review is given in: P. Prelovšek and J. Bonča, *Ground State and Finite Temperature Lanczos Methods in Strongly Correlated Systems*, Solid-State Sciences **176** (Springer, Berlin, 2013).
 - ⁴⁹ M. Mierzejewski and P. Prelovšek, Phys. Rev. Lett. **105**, 186405 (2010).
 - ⁵⁰ R. Steinigeweg *et al.*, Phys. Rev. B **85**, 214409 (2012).
 - ⁵¹ J. V. Alvarez and C. Gros, Phys. Rev. Lett. **88**, 077203 (2002).
 - ⁵² S. Grossjohann and W. Brenig, Phys. Rev. B **81**, 012404 (2010).
 - ⁵³ S. Langer *et al.*, Phys. Rev. B **79**, 214409 (2009).
 - ⁵⁴ S. Jesenko and M. Žnidarič, Phys. Rev. B **84**, 174438 (2011).
 - ⁵⁵ C. Karrasch, J. H. Bardarson, and J. E. Moore, Phys. Rev. Lett. **108**, 227206 (2012).
 - ⁵⁶ C. Karrasch *et al.*, Phys. Rev. B **87**, 245128 (2013).
 - ⁵⁷ C. Karrasch, J. E. Moore, and F. Heidrich-Meisner, Phys. Rev. B **89**, 075139 (2014).
 - ⁵⁸ C. Karrasch, D. M. Kennes, J. E. Moore, Phys. Rev. B **90**, 155104 (2014).
 - ⁵⁹ Y. Huang, C. Karrasch, and J. E. Moore, Phys. Rev. B **88**, 115126 (2013).
 - ⁶⁰ C. Karrasch, R. Ilan, and J. E. Moore, Phys. Rev. B **88**, 195129 (2013).
 - ⁶¹ T. Prosen and M. Žnidarič, J. Stat. Mech.: Theory Exp. **2009**, P02035.
 - ⁶² M. Žnidarič, Phys. Rev. Lett. **106**, 220601 (2011).
 - ⁶³ O. F. de Alcantara Bonfim and G. Reiter, Phys. Rev. Lett. **69**, 367 (1992); Phys. Rev. Lett. **70**, 249 (1993).
 - ⁶⁴ R. W. Gerling and H. Leschke, Phys. Rev. Lett. **70**, 248 (1993).
 - ⁶⁵ R. Steinigeweg, EPL **97**, 67001 (2012).
 - ⁶⁶ J. Sirker, R. G. Pereira, and I. Affleck, Phys. Rev. Lett. **103**, 216602 (2009); Phys. Rev. B **83**, 035115 (2011).
 - ⁶⁷ R. Steinigeweg and R. Schnalle, Phys. Rev. E **82**, 040103R (2010).
 - ⁶⁸ R. Steinigeweg, Phys. Rev. E **84**, 011136 (2011).
 - ⁶⁹ P. Jung, R. W. Helmes, and A. Rosch, Phys. Rev. Lett. **96**, 067202 (2006).
 - ⁷⁰ P. Jung and A. Rosch, Phys. Rev. B **76**, 245108 (2007).
 - ⁷¹ K. De Raedt *et al.*, Comp. Phys. Comm. **176**, 121 (2007).
 - ⁷² F. Jin *et al.*, J. Phys. Soc. Jpn. **79**, 124005 (2010).
 - ⁷³ A. Kolezhuk and H. Mikeska, Lect. Not. Phys. **645**, 1 (2004).
 - ⁷⁴ R. Kubo, M. Toda, and N. Hashitsume, *Statistical Physics II: Nonequilibrium Statistical Mechanics* (Springer, Berlin, 1991).
 - ⁷⁵ J. M. P. Carmelo, T. Prosen, and D. K. Campbell, preprint, arXiv:1407.0732 (2014).
 - ⁷⁶ For $\Delta = 0$, the XXZ Hamiltonian describes a model of free spin-less fermions, $H = J \sum_{i=1}^L \cos(2\pi i/L) n_i$, where the single-particle dispersion consists of only L points at positions $2\pi i/L$. Thus, for finite L , the spectrum of any correlation function in the vicinity of $\Delta = 0$ is necessarily sparse and, except for trivial cases, has to feature strong finite-size effects, e.g., even-odd effects.